GEOCHRONOMETRIA 51 (2024) 189750
DOI 10.20858/geochr/189750

Available online at https://www.geochronometria.com/

CHRONOSTRATIGRAPHY OF THE LATE GLACIAL ŻABINKO SITE (WESTERN POLAND) AND INVESTIGATION OF THE DOSE RATE VARIABILITY

AGNIESZKA SZYMAK[1], PIOTR MOSKA[1], ROBERT J. SOKOŁOWSKI[2], GRZEGORZ PORĘBA[1] and KONRAD TUDYKA[1]

[1]Institute of Physics – Centre for Science and Education, Silesian University of Technology, Konarskiego 22B, 44-100 Gliwice, Poland
[2]Department of Geophysics, Institute of Oceanography, University of Gdańsk, al. Piłsudskiego 46, 81-378 Gdynia, Poland

Received 18 July 2023 Accepted 6 June 2024

Abstract
The Żabinko exposure (western Poland) reveals the classic fluvio-aeolian succession known from studies in the European Sand Belt. Previous chronostratigraphic studies were mainly based on uncalibrated radiocarbon dates from organic sediments and thermoluminescence dating. The picture visible from these studies indicated a number of discrepancies between these methods. The new research in this exposure was based on optically stimulated luminescence (OSL) dating and calibrated radiocarbon dates. The results obtained indicate a general discrepancy between the results achieved by these two methods. While the radiocarbon dates provide some meaningful picture and allow correlation with previous studies, the results of OSL dating do not allow for a chronological model of sedimentary processes. The OSL dates show large inversions of the results and are clearly younger than the other dating results. Detailed analysis of OSL measurements shows radioactive disequilibrium and variability linked to differential stratification of sediments, significantly impacting the assessment of environmental dose rates. We believe that this atypical variability is presumably the result of postdepositional processes, such as changes in groundwater levels, chemical weathering and radionuclide migration.

Keywords
Fluvio-aeolian succession, Luminescence dating, Radiocarbon dating, Radioactive disequilibrium

1. Introduction

A reliable stratigraphic scheme of sedimentary successions is one of the crucial elements in palaeoenvironmental reconstructions. Earth sciences have numerous methods of geochronology performance, appropriate for different types of depositional environments. For Quaternary terrestrial deposits one of the most important are radiocarbon methods for organic material and luminescence methods for clastic deposits (Brauer *et al.*, 2014). Both methods have specific limitations related to features of studied deposits (Hughes *et al*., 2016; Kalińska *et al*., 2023). One of the most important limitations of the radiocarbon method is its time range, not exceeding 50–60 ka. Therefore, luminescence methods are particularly useful for frequently presenting fluvial and aeolian deposits, where organic material is not widely observed or is redeposited from older successions (Bateman, 2008).

Fluvio-aeolian succession is widespread in the European Sand Belt (Zeeberg, 1988; Kasse, 2002). This succession reflects the main and even short-time environmental changes, related to climate and base-level changes noted in the Late Pleistocene (Crombé *et al*., 2020; Sokołowski *et al*., 2022). Fluvial and especially aeolian deposits have a great potential to be dated using luminescence methods due to their potentially long exposure on sunlight and well bleaching and high percentage of quartz grains in sand fraction. In the last years, there has been a significant increase in luminescence dating, leading to the establishment of more precise and detailed stratigraphic schemes. Most of dating results were obtained using optically stimulated luminescence (OSL). Nevertheless, a comparison of

Corresponding author: A. Szymak
e-mail: Agnieszka.Szymak@polsl.pl

ISSN 1897-1695 (online), 1733-8387 (print)

luminescence dating results in particular profiles reveal sometimes significant inversions (Fitzsimmons *et al*., 2007; Pincé *et al*., 2022). Also, in profiles, where organic material suitable for radiocarbon dating is present, some discrepancies between both methods are observed.

Detailed studies of luminescence dating results, where inversions or discrepancies between radiocarbon and OSL results are present, reveal that OSL measurements have unimodal and sharp peaks. It means that material was well bleached and the problem with reliable results is elsewhere. It is particularly visible in profiles, where the youngest OSL dating results are located in the lowermost part of the investigated profiles (Moska *et al*., 2022). Field observations suggest that it is connected to the changes of ground water level. This assumption leads to preliminary conclusion that the dose rate might be over- or underestimated in relation to geological history of investigated fluvio-aeolian successions. Therefore, the following questions arise: (i) is it possible to establish an internally consistent chronotratigraphic model and its correlation with previous research results and the general fluvio-aeolian succession model; (ii) is there any relation between the lithological heterogeneity of the studied sediments and differences in radioactivity; (iii) what type of disequilibrium in radionuclide activity might exist in the studied sediments and what might be the reasons for this?

To answer the research questions posed in this way, a profile of Żabinko, western Poland, was selected (**Fig. 1**). This profile was chosen because it had already been previously investigated in terms of the age and origin of fluvio-aeolian succession deposits (Bohncke *et al*., 1995; Kozarski and Nowaczyk, 1995; Zieliński *et al*., 2011). In the profile detailed sedimentary studies were performed. Additionally, 4 samples from palaeosols and gyttja/peat layers for radiocarbon dating as well as 15 samples for OSL dating were collected (**Fig. 2**).

2. Geological setting and previous studies

The Żabinko outcrop is located in the active open sand pit in the central and distal parts of compound parabolic dunes circa 20 km towards the south from Poznań, western Poland (**Fig. 1**). The detailed studies have been performed in two profiles. Aeolian, fluvio-aeolian, upper and central part of the fluvial complexes were studied in the profile I and lower part of the fluvial complex superimposed by lacustrine sediments were studied in the profile II. Profile I was made in the outcrops' wall while profile II has been dug up in the bottom of the outcrop up to the ground-water level. Both profiles were located several metres from each other and reveal continued succession. Integrated profile is presented in the **Fig. 2**.

The dune complex was deposited in the Warsaw-Berlin ice-marginal valley (IMV) within the limit of the Last Glacial Maximum (Kozarski *et al*., 1988). The Warsaw-Berlin IMV formed during melt-water outflow towards the west along the ice margin. In the result of outflow an accumulation terrace with sands and gravels was formed. At the very end of the Late Pleniglacial a formation of the Warta River system outflow towards the north took place and multi-channel fluvial system functioned. It transformed from a braided system to anastomosing system and then in the Bølling interstadial to meandering fluvial system (Bohncke *et al*., 1995; Kozarski and Nowaczyk, 1995).

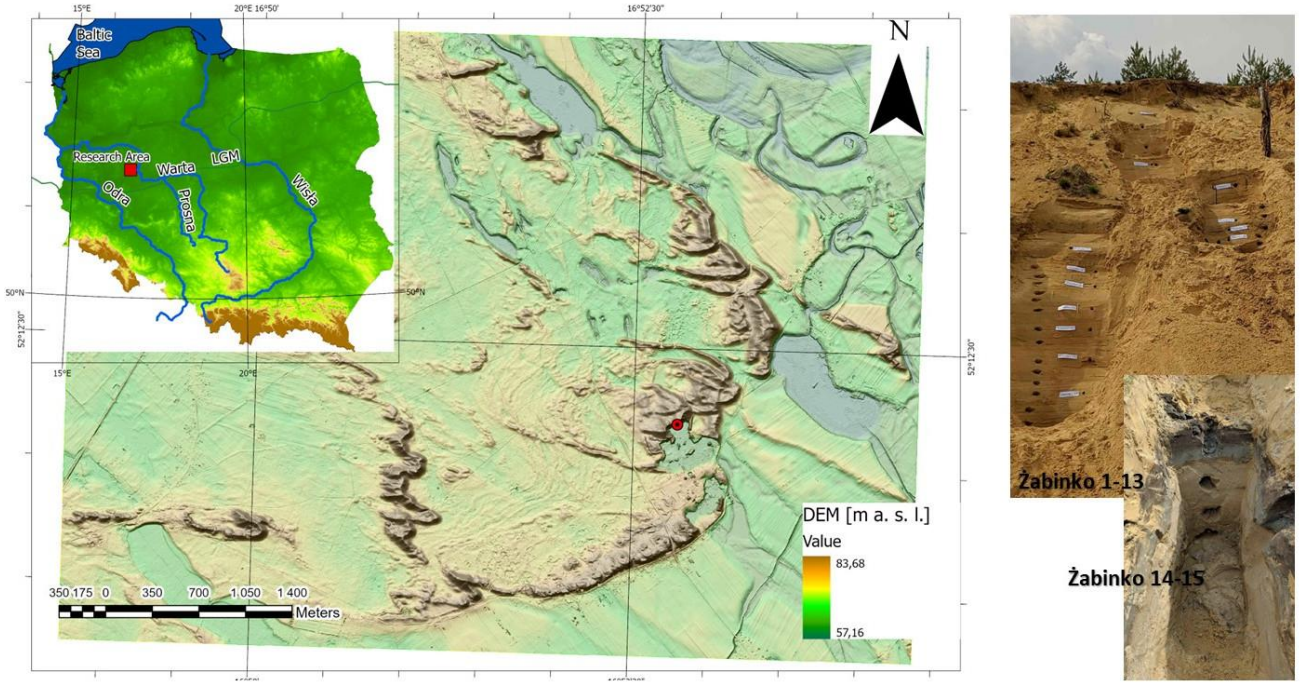

Fig. 1. *The location map of the study area and two profiles in the Żabinko site.*

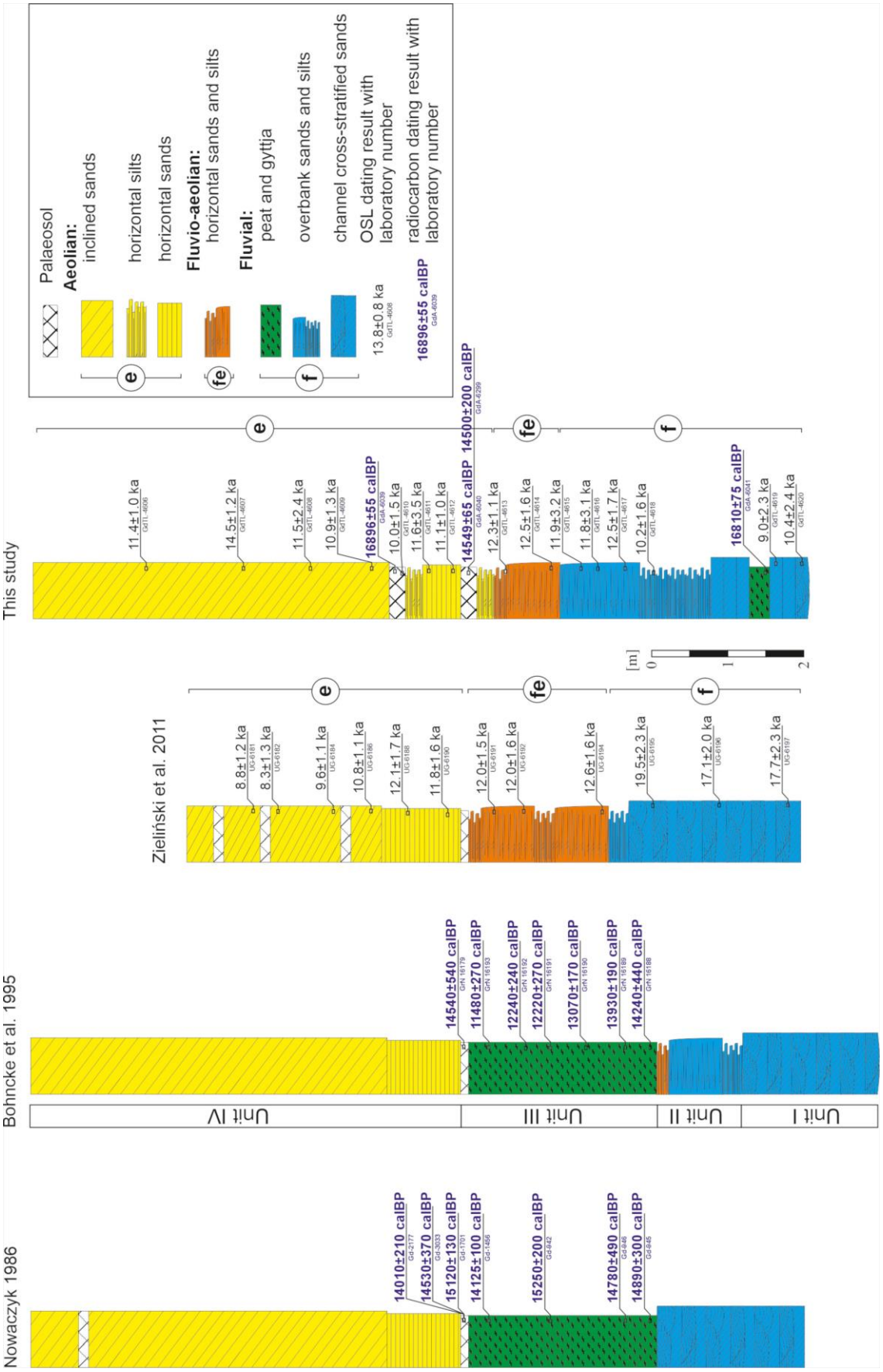

Fig. 2. *Correlation of previous studies results with these studies from the Żabinko site.*

The first studies of aeolian series in the Żabinko site was published by Nowaczyk (1986). He identified deflation depression, aeolian sand covers and parabolic dunes with well-developed southern branches. The compound parabolic dunes reach 3 km in lateral range and 20 m in the highest points of dune foresets. Below the dune complex of braided river channels was identified, locally infilled with organic material. The calibrated radiocarbon dating results reveal that the infilling of abandoned channel started at the final part of the Late Pleniglacial (the Oldest Dryas in the biostratigraphic scheme, GS-2.1a in Greenland scheme; Rasmussen *et al*., 2014) and continued at least to the final part of the Bølling interstadial (GI-1e; **Fig. 2**). The calibrated radiocarbon dating results obtained from the palaeosols reveal comparable age (15120 ± 130 calBP – 14010 ± 210 calBP, **Fig. 2**). In the northern part of the study area the distal part of the dune complex is situated on the edge of subglacial through of generally north-south axis with several lakes, among others by Baranówko Lake (**Fig. 1**).

Studies of Bohncke *et al.* (1995) and Kozarski and Nowaczyk (1995) reconstructed palaeoenvironmental conditions during the depositional processes and established stratigraphic scheme at the basis of uncalibrated radiocarbon dating results combined with palynological analysis. The calibrated radiocarbon dates and the generalised profile from the aforementioned authors' study are shown in **Fig. 2**. Four depositional units were identified: I) unit I – medium to- coarse-grained sands deposited in the channel zone of the braided fluvial system during the Warsaw-Berlin IMV formation in the Late Pleniglacial (*ca.* 20–17 ka BP); ii) unit II – fine and silty sands and silts with alternating ripple-cross lamination and wavy lamination. This unit was identified as a continuum of the Unit I fluvial depositional processes in the flood-plain zone. In the lower part of the unit II and in the unit I syngenetic-ice-wedge casts were identified and interpreted as permafrost remnants. The upper part of the unit II consists of alternating bedding of fine-grained sands and silts with crinkly lamination, wavy lamination and low-angle-cross stratification. It was interpreted as fluvio-aeolian deposition *sensu stricte* (Kasse, 2002); iii) unit III is composed of 4 m thick lacustrine deposits (peat and gyttja) deposited in the abandoned river channel. Calibration od radiocarbon dating results let to state that the unit III started to be deposited from the Bølling interstadial to the onset of the Holocene (from 14240 ± 440 calBP to 11480 ± 270 calBP, **Fig. 2**). Laterally, in the intra-channel higher located zone, a soil was formed. The soil was classified as gleyic/haplic arenosol, according to FAO (1988) classification. One calibrated radiocarbon dating result situates its age in the Bølling interstadial (14540 ± 540 calBP, **Fig. 2**); iv) unit IV consists of two types of deposits – lower is composed of silty-sandy horizontally bedded layer with wavy and crinkly lamination up to 1 m thick. Upper part represents mainly inclined sands in a large scale of the dune lee-slope.

The fluvio-aeolian succession in the Żabinko site was studied as well by Zieliński *et al*. (2011, 2015). They identified three main sedimentary complexes of the succession (**Fig. 2**) and performed thermoluminescence dating from all units (**Fig. 2**). They concluded that the fluvial complex was deposited in the Pleniglacial, at the very end of the Pleniglacial (the Oldest Dryas) fluvio-aeolian processes predominated, and aeolian activity occurred in the Older and Younger Dryas. Pedogenic processes developed in the Bølling and Allerød interstadials.

3. Materials and methods

The detailed studies were carried out in the fresh walls of the sand pit and in the crop-out in the floor up to the ground-water level. The walls were cleaned, measured and photographed to document sedimentary structures and points of sampling. The studies were to determine the lithological characteristics of the sediments (texture, structure, including structural directional elements, grain size distribution). Periglacial structures and palaeosols were also studied. The lithofacies analysis was based on the methodology proposed for fluvial sediments by Miall (1996) with subsequent modifications (Zieliński; 1998, 2014) and for aeolian sediments according to Zieliński (2016). Samples to establish their chronostratigraphic positions (OSL and ^{14}C dating) were collected from all lithofacial complexes (**Fig. 3**). The sediment for OSL analysis was collected to the thin-walled pipes (material for quartz extraction) and into the plastic bags (bulk material for another research).

At the Gliwice Luminescence Dating Laboratory (Moska *et al*., 2021), samples from Żabinko were subjected to OSL dating (**Fig. 4**). In addition, further research was conducted to investigate crucial aspects for this profile such as radioactive disequilibrium, ^{222}Rn emanation which we use as a proxy for radionuclides mobility, and sample homogeneity.

3.1 Determination of luminescence age

3.1.1 Chemical procedure

To determine the equivalent dose rates from the extracted pure quartz grains a series of chemical treatments were performed. Initially, the material was immersed in 20% hydrochloric acid to remove carbonates, followed by immersion in 20% hydrogen peroxide to eliminate organic matter. Between these two steps, the samples were rinsed with distilled water. After the initial preparation, samples were dried and sifted using 125–200 μm sieves. Quartz grains were then separated using sodium polytungstate solutions – a heavy liquid of densities 2.62 and 2.75 $g \cdot cm^{-3}$. Subsequently, the grains were etched in 40% hydrofluoric acid for 1 hour to remove the outer layer of approximately 4 μm, which is responsible for the partial absorption of external alpha radiation dose (Poręba *et al*., 2022), and to eliminate non-quartz components. The prepared sample

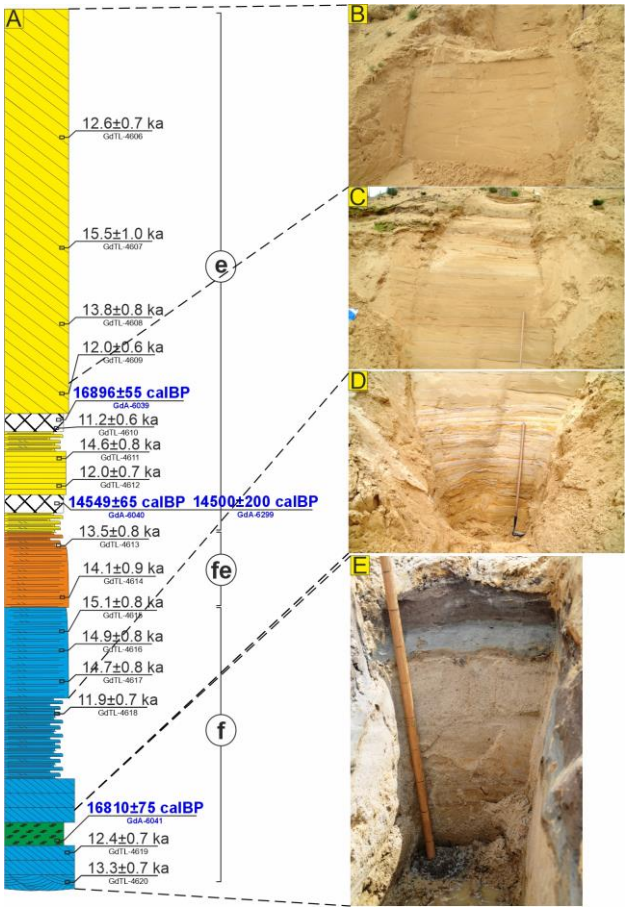

Fig. 3. *A – the sedimentary log with radiocarbon/OSL dating results; B – upper part of the aeolian complex with inclined-cross stratification; C – lower part of the aeolian complex with two palaeosols, silty-sandy deposits of the fluvio-aeolian complex and fine sands and sandy silts of the fluvial complex; D – central part of the fluvial complex with silty-clayey rhythmite; E – sands of the abandoned fluvial channel overlaid by gyttja (light grey) and sandy peat (dark grey).*

was then placed on stainless steel disks and subjected to the procedure described in the following paragraph.

3.1.2 Equivalent dose rate determination

The luminescence measurements were carried out using Risø TL/OSL DA-20 automatic reader equipped with Hoya U-340 filter and calibrated $^{90}Sr/^{90}Y$ beta source. In calibration process Riso quartz was used (Autzen *et al*., 2022). For determining equivalent doses, the SAR protocol (Single-Aliquot Regenerative-dose) (Murray and Wintle, 2000) was applicated and for each tested sample the final value of the equivalent dose was calculated by implemented the Central Age Model (CAM) (Galbraith *et al*., 1999).

3.1.3 Dose rate determination

HPGe high resolution spectrometry

The natural uranium, thorium decay chains and potassium were measured using a high-resolution gamma HPGe detector. The HPGe detector was calibrated for *ca.* 100 g samples using reference materials *i.e.*, IAEA-RGU-1, IAEA-RGTh-1, and IAEA-RGK-1 from the International Atomic Energy Agency.

Samples were dried at 70°C, sealed in γBeakers (Poręba *et al*., 2020) and immediately measured on HPGe detector. After the initial measurements samples were re-measured after more than 3 weeks. The activities were determined using the following gamma lines: 1460.8 keV for ^{40}K, 583 keV, 911.2 keV, and 2614.4 keV for ^{232}Th, 63.3 keV for ^{234}Th, 295.1 keV, 352.0 keV, 609.3 keV, and 1120.3 keV for ^{226}Ra, and 46.5 keV for ^{210}Pb. Both measurements ^{234}Th and ^{210}Pb were corrected for self-absorption according to Cutshall *et al.* (1983). Ra-226 was determined by using the secular equilibrium, and gamma lines from the ^{214}Pb and ^{214}Bi.

µDose measurement

In addition, the µDose system (Tudyka *et al*., 2018) was used to measure natural uranium, thorium decay chains, and potassium. The system was calibrated using IAEA-RGU-1, IAEA-RGTh-1, and IAEA-RGK-1 standards from the International Atomic Energy Agency. For this type of research, 3.00 grams of the dried and ground sample was evenly distributed on a 7 cm diameter sample holder and placed in a container. The µDose system measures gross alpha and beta counts, and as the conversion factors for dose rates do not exhibit significant changes per count (Sanderson, 1988), it was used to assess the limits on dose rates in samples that are in disequilibrium.

Dose rate calculation

The alpha efficiency was assessed with a value of 0.04 ± 0.02, and the dose rate was corrected for water content according to Aitken (1985). The water content was determined to be $7 \pm 3\%$ (Żabinko 1–9), $10 \pm 3\%$ (Żabinko 10–13) and $20 \pm 5\%$ (Żabinko 14 and 15), which was established on the basis of sediment type and environmental conditions (according to the assumption). To account for the etched away layer of 4 ± 2 µm, we utilized data proposed by Bell (1979) and Brennan (2003). Additionally, for the correction of radiation attenuation in quartz grains (the 125–200 µm fraction), we referred to the data provided by Brennan *et al.* (1991) for the alpha correction and Guérin *et al.* (2011) for the beta correction. The cosmic dose rate was determined following the methodology presented by Prescott and Hutton (1994).

Furthermore, the calculations took into account the disequilibrium present and in the profile and the indication of material non-homogeneity through lamination (refer to **Fig. 3**). This we had assessed by allowing to parts of decay chain *i.e.* ^{238}U - ^{266}Ra and ^{222}Rn-^{206}Pb to change by a factor of 1 in the µRate software. Next, dose rates from the HRGS and µDose systems were averaged and we added mean difference to the uncertainty, to provide more realistic uncertainty. In addition, we added mean internal dose rate from Szymak *et al.*, (2022) for Żabinko as several have low radioactivity. This approach reduced scattering of ages as

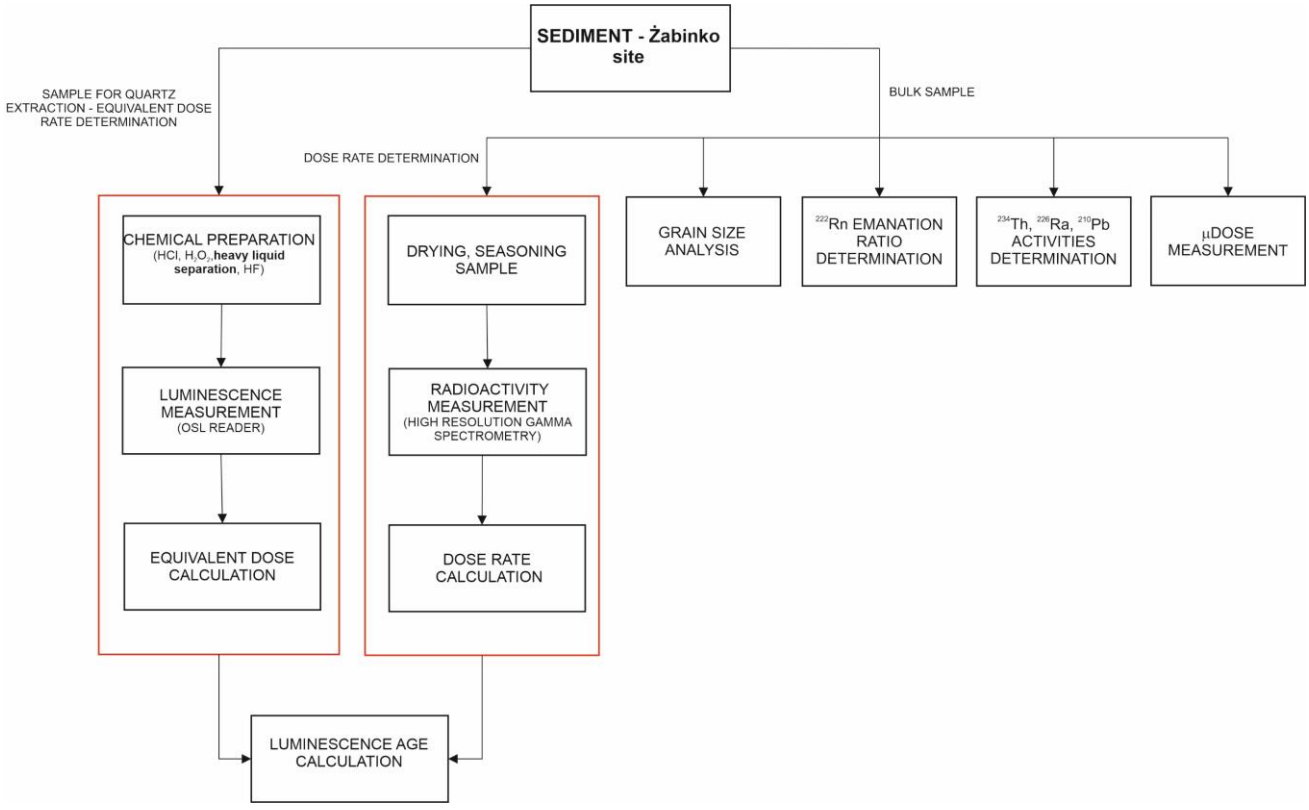

Fig. 4. *Research methodology for Żabinko site.*

well uncertainties do not exhibit significant age inversions. Consequently, we calculated the mean and average dose rate offset between the HRGS and µDose systems. Although this approach significantly increases the uncertainty in the dose rates, it provides more reliable estimates that consider the aforementioned factors.

The dose rates were calculated using the online software µRate (Tudyka *et al*., 2022). **Table 1** includes the key data for the investigated samples, such as sample names, depths, water contents, radionuclide activity, dose rates, equivalent dose rates, and final ages.

3.2 Additional research

3.2.1 Radiocarbon dating

Graphite targets were prepared in the Gliwice ^{14}C Laboratory and ^{14}C concentration was measured using Accelerator Mass Spectrometry (AMS). Before radiocarbon dating all tested samples (sediment material) were subjected to chemical treatment based on NaOH-SOL procedure. In the first step, the sample was immersed in 0.5 M HCl and heated in a water bath at 85°C for 1 hour. Then, it was rinsed with deionized water to achieve a neutral pH. Next, the sample was immersed in 0.1 M NaOH solution under the same conditions. Again, it was rinsed with deionized water to reach a neutral pH. Afterward, the cooled solution above the sediment was neutralized with 0.5 M HCl. This fraction is referred to as the NaOH solution. All ^{14}C ages were calibrated using OxCal software v.4.4.4 (Bronk Ramsey, 2009) and the IntCal2020 calibration curve (Reimer *et al*., 2020). All the ^{14}C results are included in the **Table 2**.

3.2.2 Grain size analysis

Grain-size distributions were analysed using a Malvern Mastersizer 3000 laser diffractometer. Prior to the measurement, organic matter was eliminated using H_2O_2. To disperse the samples, sodium hexametaphosphate was added, and samples were shaken overnight in distilled water (Mason *et al*., 2003).

The results of grain-size analysis along with depth are presented in **Fig. 5**. The grain size results are presented as cumulative curves, as well as in the form of mean and median particle sizes. Within the profile, strong variations in the mean and median grains diameter as well as the proportions of grains size fractions are observed. In the upper part of the studied profile, a depletion in the fraction 16–63 µm compared to the rest is observed, while the proportion of grains above 250 µm increases. On the other hand, the lower part of the profile shows an increase in the proportion of fractions above 250 µm.

Table 1. *All important data for investigated samples: samples names, depth, water content, radionuclid activity (HRGS), dose rate – HRGS (assuming secular equilibrium, homogeneous infinite matrix and no internal dose rate), dose rate - µDose system (assuming secular equilibrium, homogeneous infinite matrix and no internal dose rate), final dose rate (taking into account fact that profile is not homogenius, radioactive disequiloibrium and internal dose rate), equivalent dose rate and OSL age.*

Lab. Code	Sample ID	Sampling depth (cm)	H_2O (%)	^{232}Th (Bq·kg^{-1})	^{226}Ra (Bq·kg^{-1})	^{40}K (Bq·kg^{-1})	Dose rate – HRGS (Gy·ka^{-1})	Dose rate – µDose system (Gy·ka^{-1})	Final dose rate (Gy·ka^{-1})	Equivalent dose (Gy)	OSL age (ka)
GdTL_4606	Żabinko_1	150	7 ± 3	4.1 ± 0.5	5.5 ± 0.3	254 ± 20	1.07 ± 0.06	1.15 ± 0.05	1.20 ± 0.10	13.7 ± 0.3	11.4 ± 1.0
GdTL_4607	Żabinko_2	280	7 ± 3	3.2 ± 0.4	3.5 ± 0.3	223 ± 17	0.91 ± 0.05	0.89 ± 0.04	0.99 ± 0.07	14.3 ± 0.5	14.5 ± 1.2
GdTL_4608	Żabinko_3	370	7 ± 3	4.7 ± 0.4	4.0 ± 0.2	240 ± 18	0.98 ± 0.05	1.22 ± 0.05	1.18 ± 0.24	13.6 ± 0.4	11.5 ± 2.4
GdTL_4609	Żabinko_4	440	7 ± 3	10.3 ± 0.6	13.2 ± 0.5	360 ± 28	1.55 ± 0.08	1.75 ± 0.07	1.75 ± 0.20	19.0 ± 0.4	10.9 ± 1.3
GdTL_4610	Żabinko_5	470	7 ± 3	14.7 ± 0.7	17.1 ± 0.6	416 ± 32	1.83 ± 0.09	2.17 ± 0.09	2.10 ± 0.31	21.0 ± 0.5	10.0 ± 1.5
GdTL_4611	Żabinko_6	510	7 ± 3	4.5 ± 0.5	5.6 ± 0.3	261 ± 20	1.04 ± 0.06	1.44 ± 0.07	1.33 ± 0.40	15.4 ± 0.3	11.6 ± 3.5
GdTL_4612	Żabinko_7	550	7 ± 3	14.2 ± 0.7	14.0 ± 0.5	384 ± 29	1.67 ± 0.08	1.83 ± 0.08	1.85 ± 0.15	20.6 ± 0.5	11.1 ± 1.0
GdTL_4613	Żabinko_8	630	7 ± 3	6.0 ± 0.4	7.2 ± 0.3	303 ± 23	1.20 ± 0.06	1.28 ± 0.06	1.33 ± 0.11	16.4 ± 0.6	12.3 ± 1.1
GdTL_4614	Żabinko_9	670	7 ± 3	7.2 ± 0.4	7.3 ± 0.3	326 ± 25	1.28 ± 0.07	1.46 ± 0.06	1.46 ± 0.18	18.3 ± 0.5	12.5 ± 1.6
GdTL_4615	Żabinko_10	720	10 ± 3	7.9 ± 0.5	7.9 ± 0.3	248 ± 19	1.03 ± 0.05	1.43 ± 0.06	1.34 ± 0.36	15.9 ± 0.3	11.9 ± 3.2
GdTL_4616	Żabinko_11	760	10 ± 3	5.9 ± 0.4	6.7 ± 0.3	272 ± 21	1.06 ± 0.05	1.44 ± 0.06	1.35 ± 0.35	15.9 ± 0.3	11.8 ± 3.1
GdTL_4617	Żabinko_12	790	10 ± 3	5.5 ± 0.5	6.8 ± 0.3	260 ± 20	1.02 ± 0.05	1.20 ± 0.05	1.21 ± 0.16	15.1 ± 0.3	12.5 ± 1.7
GdTL_4618	Żabinko_13	830	10 ± 3	9.4 ± 0.6	10.6 ± 0.4	374 ± 28	1.44 ± 0.07	1.76 ± 0.07	1.72 ± 0.27	17.5 ± 0.6	10.2 ± 1.6
GdTL_4619	Żabinko_14	950	20 ± 5	5.0 ± 0.4	5.3 ± 0.3	218 ± 17	0.77 ± 0.04	1.13 ± 0.05	1.08 ± 0.28	9.7 ± 0.3	9.0 ± 2.3
GdTL_4620	Żabinko_15	990	20 ± 5	5.4 ± 0.4	6.5 ± 0.3	230 ± 18	0.82 ± 0.05	1.11 ± 0.05	1.07 ± 0.24	11.2 ± 0.3	10.4 ± 2.4

4. Results and discussion

4.1 Sedimentary studies

The sedimentary studies were carried out in two neighbouring profiles in close proximity to each other (about 5 m) and reflect continuous succession. Three main lithofacial complexes were distinguished, according to sedimentary model proposed by Zieliński *et al*. (2011). Lower, fluvial complex consists of two lithofacial associations related to channel and overbank sedimentary zones. The channel association was located in the lowermost part of the profile and consists of cross-stratified medium- and coarse-grained sands with thin mud intercalations. In the upper part of this association 30 cm thick detritus gyttja and sandy peat was observed (**Fig. 3A**). From this association two samples for OSL and two for radiocarbon dating were collected. Above the gyttja-peat layers the 2.5 m thick overbank association was observed. It consists of rhythmite of fine-grained sands with ripple-cross lamination intercalated with silts and thin clay laminae with wavy, flaser and horizontal lamination (**Fig. 3B**). From this association four samples for OSL dating were taken. Above the fluvial deposits a middle, 1 m thick, fluvio-aeolian complex was distinguished. It consists of sands and silty sands with ripple-cross and adhesion ripple lamination, flaser lamination and massive structure, and medium-grained sands with tabular cross-stratification of medium scale and horizontal stratification (**Fig. 3C**). The uppermost, aeolian complex is over 6 m thick and consists of two lithofacial associations (**Fig. 3D**). Lower association cover directly fluvio-aeolian complex and consists of low-angle to horizontal stratified middle-grained sands separated with two layers of gleyed sandy silts reworked by soil processes. In the upper palaeosol occur several thin, discontinuous humus streaks overlying strongly gleyed silty-sandy deposits (**Fig. 3E**). The upper aeolian association is composed of high-angle inclined stratified medium- to coarse grained sands (**Fig. 3E**).

4.2 Radioactivity measurements and dose rate determination

The results of the radionuclide contents of the bulk samples are presented in **Table 1**, where relatively high variability of ^{226}Ra, ^{232}Th and ^{40}K content can be noticed. The calculated relative standard deviation (RSD) for ^{226}Ra and ^{232}Th is 48.6% and 48.8% respectively, while for ^{40}K is significantly lower at 22.2%. Similar results are obtained for activities obtained by µDose. The RSD for the calculated dose rate is 25.6%. In the vertical distribution of ^{226}Ra and ^{232}Th activities, three distinct areas of increased activity are noticeable at depths 440–470 cm, around 550 cm, and around 830 cm. Similar increases in activity can be observed for ^{40}K, although with significantly smaller percentage differences compared to ^{226}Ra or ^{232}Th. The correlation between the obtained activity values for ^{226}Ra, ^{232}Th,

Table 2. *^{14}C results after calibration.*

Lab. Code	material	^{14}C age calBP Probability 95.4%	^{14}C age calBP
GdA_6039	sediment	17146 – 16646	16896 ± 55
GdA_6040	sediment	14932 – 14166	14549 ± 65
GdA_6041	sediment	17100 – 16520	16810 ± 75
GdA_6299	sediment	15096 – 14770 or 14717 – 14322	14500 ± 200 or 14900 ± 200
Gd_942	twigs	15797 – 14780	15250 ± 200
Gd_945	peat with plant macroremains	15500 – 14286	14890 ± 300
Gd_946	peat with plant macroremains	15776 – 13788	14780 ± 490
Gd_1456	wood	14630 – 13797	14125 ± 100
Gd_1701	peat with plant detritus	15433 – 14823	15120 ± 130
Gd_2177	peat with plant detritus	14562 – 13740	14010 ± 210
Gd_3033	peat with plant detritus	14913 – 14161	14530 ± 370
GrN_16179	mammal rib bone	15636 – 13573	14540 ± 540
GrN_16188	sandy black gyttja	15154 – 13581	14240 ± 440
GrN_16189	fine detrital gyttja	14801 – 14716	13930 ± 190
GrN_16190	sandy coarse detr. gyttja	13360 – 12760	13070 ± 170
GrN_16191	brown peat	12724 – 11689	12220 ± 270
GrN_16192	dark brawn, sandy peat	12624 – 11823	12240 ± 240
GrN_16193	amorphous peat	11749 – 11210	11480 ± 270

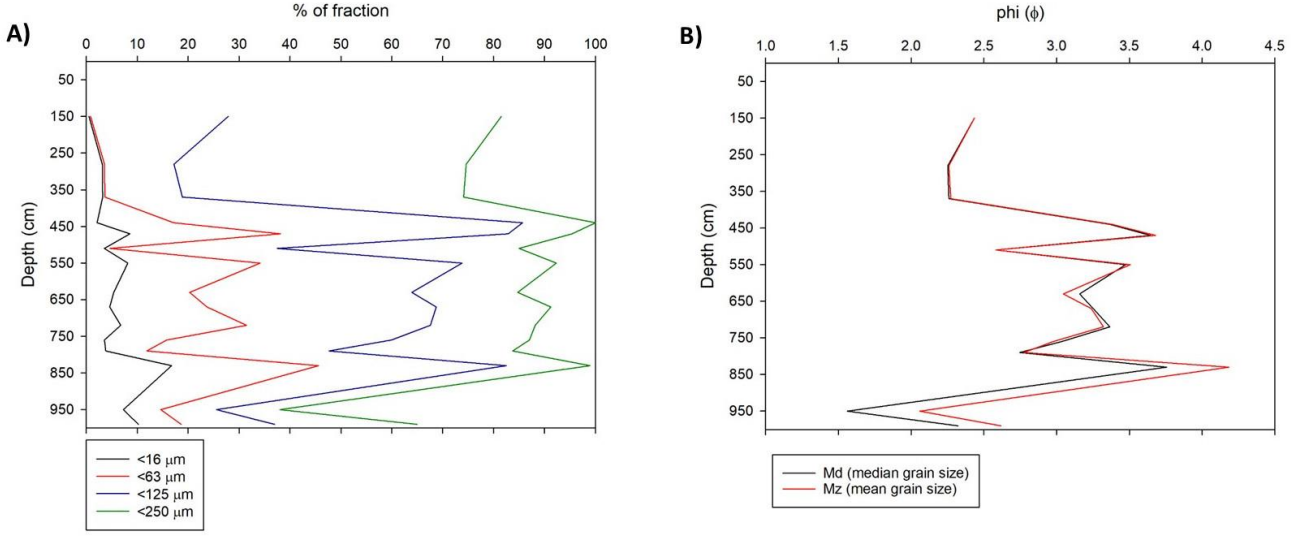

Fig. 5. *Grain size analysis. A – the changes in grain size distribution of the sample with depth; B – the changes in the median and mean grain size from the Żabinko site.*

^{40}K and the fraction below 16 µm is relatively weak, while a significantly stronger correlation is observed with the 16–63 µm fraction, as well as with the mean grain size.

In the **Fig. 6** activity for ^{234}Th, ^{226}Ra (via ^{214}Bi, ^{214}Pb) and ^{210}Pb is shown. In the case of ^{234}Th, the general pattern of changes of activity in the profile is quite similar to changes ^{226}Ra activity. However, discrepancies can be observed in the upper and lower parts of the profile, where ^{234}Th activity visibly increases. On the other hand, ^{210}Pb exceeds the activity of ^{226}Ra in part of samples, notably at the depth range 670–760 cm, where the differences are quite significant. Moreover, the measurement conducted immediately after the sample preparation and after equilibrium between radon and its progeny, allowed us to obtain ^{222}Rn emanation for dry material (**Fig. 6**). The calculated values of radon emanation for the studied samples ranged from 11% to 25% for dried sediment samples. In the natural environment, it is expected that the emanation will be 2–6 times higher due to the presence of water (Strong and Levins, 1982). Moreover, strong ^{222}Rn emanation suggests

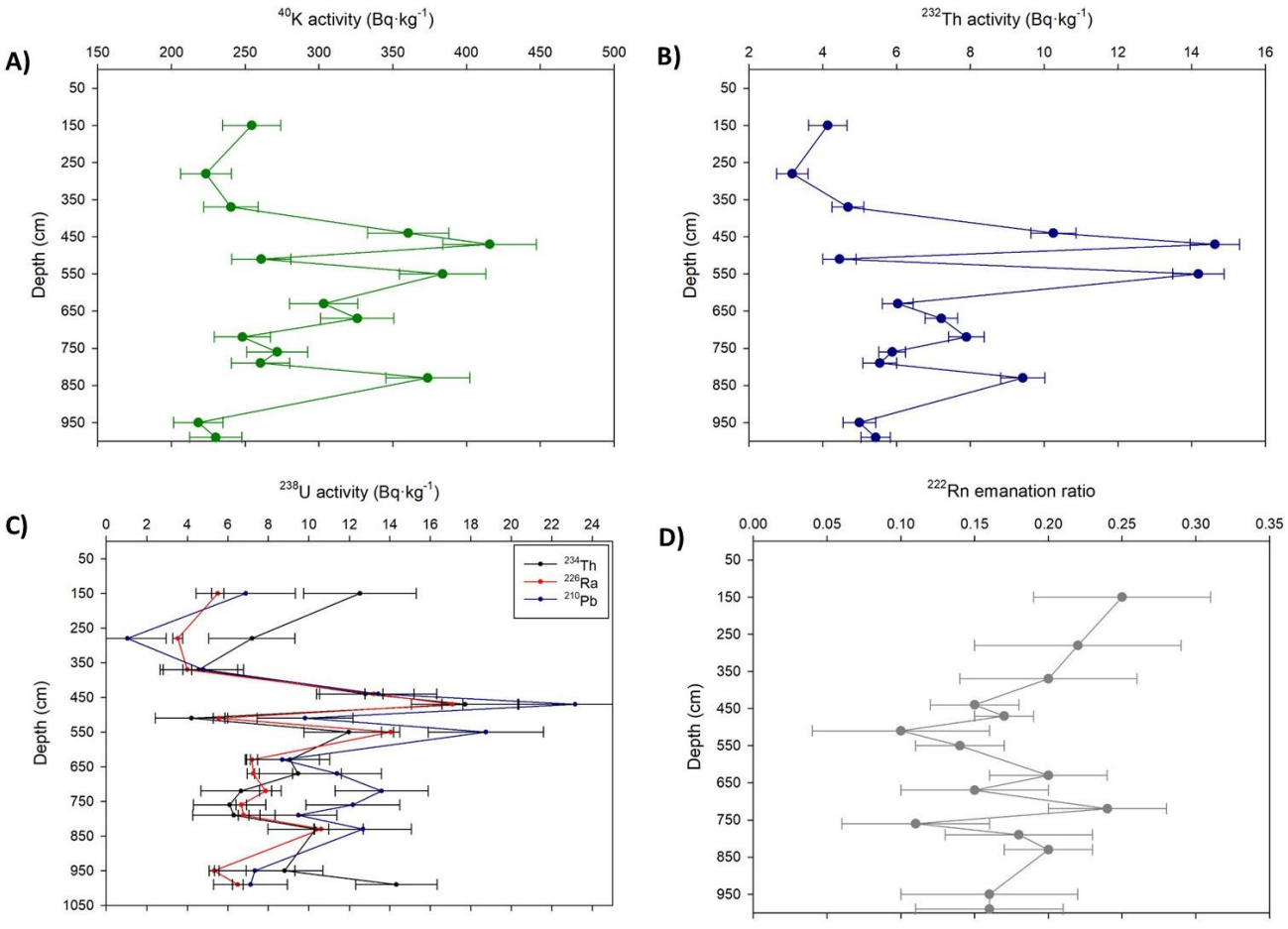

Fig. 6. *Radionuclides (A–C) and radon emanation factor (D) in Żabinko site. Potasium-40 activity (A), activities of ^{232}Th decay chain (B) and radionuclides of ^{238}U decay chain (C).*

that other radionuclides from ^{226}Ra subseries can be mobilized in the Żabinko profile.

The activities of ^{234}Th, ^{226}Ra, and ^{210}Pb, as well as radon emanation, indicate disequilibrium in the ^{238}U series. Although the uncertainty in ^{234}Th and ^{210}Pb measurements is relatively high, only in 4 out of 15 samples did the radioactivity of ^{234}Th, ^{226}Ra, and ^{210}Pb vary within 1 standard deviation. On average, the activity ratio of ^{234}Th to ^{226}Ra is 1.28, similarly, the activity ratio of ^{210}Pb to ^{226}Ra is 1.3. In addition, dose rates values obtained with µDose system are also systematically increased compared to values obtained from ^{226}Ra estimates from HRGS this again suggests presence of disequilibrium. Moreover, considering the half-lives of individual radionuclides, especially ^{210}Pb, it can be inferred that the change in ^{226}Ra activity could have occurred relatively recently, within the past several decades to a hundred years.

4.3 OSL and ^{14}C measurement

The luminescence results are presented in the form of graphs of the probability density distribution (**Fig. 7**). Overdispersion parameter for all samples was much lower than 20% and distributions are unimodal, therefore can be assumed that the tested material represent group of the well-bleached quartz (Moska, 2019) and CAM model can be applied for final equivalent doses calculation.

The minimum and maximum values of equivalent dose were observed for Żabinko 14 (GdTL-4619) and Żabinko 5 (GdTL-4610) respectively. The chronology presented in **Fig. 2** and **Fig. 3A** includes the OSL results. In the aeolian complex, we obtained dates ranging from 10.0 ± 1.5 ka (GdTL-4610) to 14.5 ± 1.2 ka (GdTL-4607). For the middle complex (fluvio-aeolian), we obtained two dates: 12.3 ± 1.1 ka (GdTL-4613) and 12.5 ± 1.6 ka (GdTL-4614). For the last section (fluvial complex), the ages range from 9.0 ± 2.3 ka (GdTL-4619) to 12.5 ± 1.7 ka (GdTL-4617). No significant age difference was found between the sample deposited at the uppermost depth (11.4 ± 1.0 ka, GdTL-4606) and the sample at the lowest depth (10.4 ± 2.4 ka GdTL-4620).

The collected material did not contain charcoal or other plant remnants; thus, the sediment was dated using radiocarbon dating. This limitation reduces the reliability of radiocarbon ages and restricts their interpretation to rough

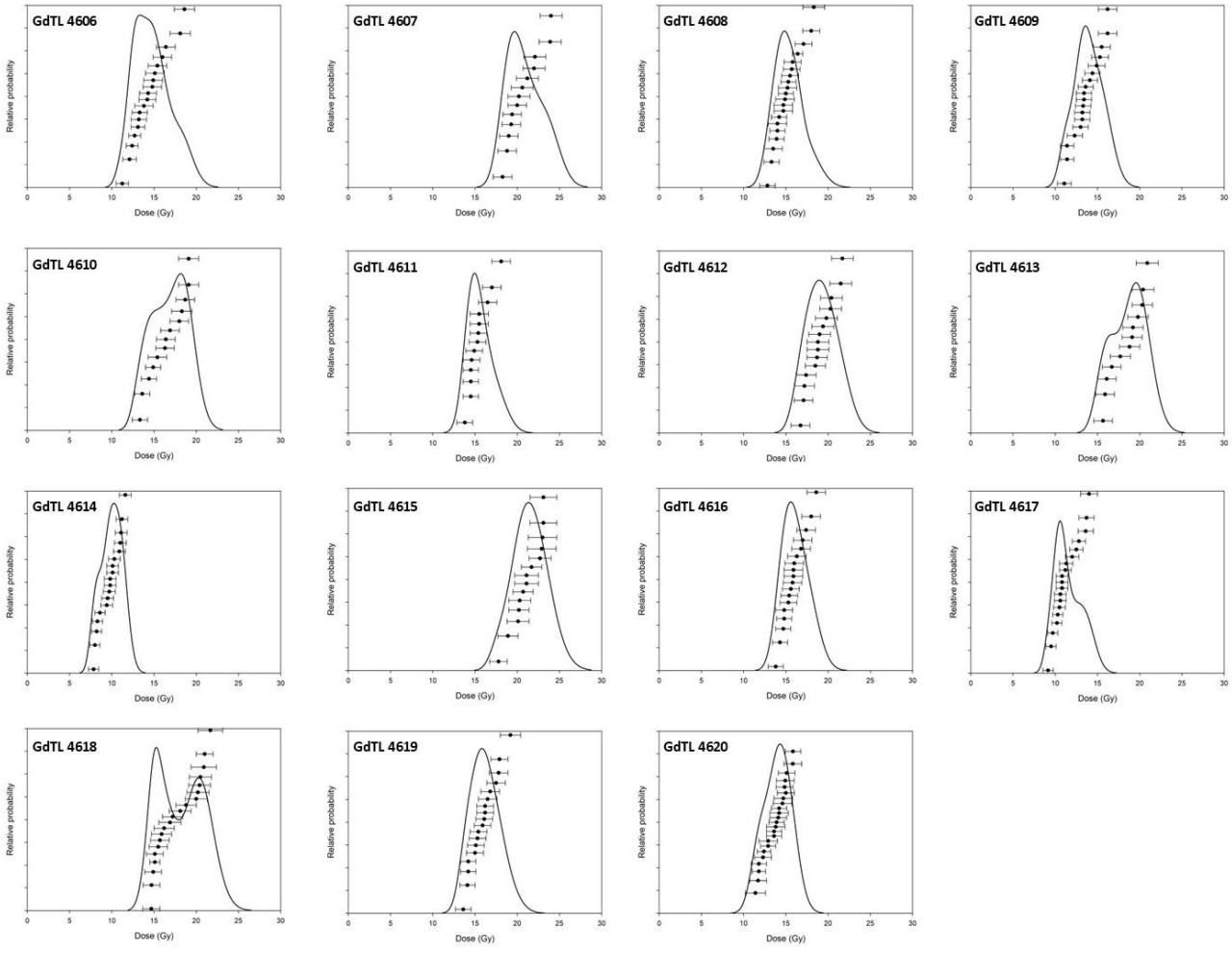

Fig. 7. *Dose distributions for all tested samples.*

estimations. ^{14}C ages were calibrated and the dates are included in the **Table 2**. The findings from ^{14}C dating indicate that the oldest samples (GdA-6039 and GdA-6041) were collected from peat and gyttja deposits, as well as from the upper palaeosol. On the other hand, the youngest samples (GdA-6040 and GdA-6299) were obtained from the lower palaeosol (**Fig. 2**).

4.4 Chronology of sedimentary processes

The obtained results of sedimentary analysis are in agreement with previous studies, particularly Zieliński *et al.* (2011). The lowermost part of the fluvial complex was deposited firstly in the channel zone of the transitional river with multiple channels (Gradziński *et al.*, 2003). The channels were abandoned due to river avulsion and then filled with organic deposits (gyttja and peat) typical for overbank deposition (Miall, 1996). The two OSL dating results from sands (9.0 ± 2.3 ka, GdTL-4619 and 10.4 ± 2.4 ka, GdTL-4620) reveal considerable reversion in comparison to other results and to previous studies, where this part of the fluvial is older than 15250 ± 200 calBP (Gd-942; Nowaczyk, 1986, **Fig. 2**) and TL dating results suggest the age of deposition at 17-19 ka (Zieliński *et al.*, 2011). The final part of infill of abandoned channel is dated on 16810 ± 75 calBP (GdA-6041). We assume that channel deposition and then subsequent organic deposition took place during the very end of the Late Pleniglacial. Due to the lateral migration of the dune and the covering of the abandoned channels fill at different times, one can see a variation in the radiocarbon dates obtained by different authors (Nowaczyk, 1986; Bohncke *et al.*, 1995). This shows the high variability of this type of environment and draws attention to the role of local factors. In this case, the main role was played by the different timing of the cover of the palaeochannels by eolian sediments

The central part of the fluvial complex represents rhythmical deposition on the floodplain (silty sand – silt/clay couplets). Such rhythmite is related to flood peak (sand/silt) and the waning of the flood wave (Benito *et al.*, 2003). The rhythmite is replaced towards the upper part of the fluvial complex by fine sands and silty sands of crevasse splay or proximal part of the floodplain (Burns *et al.*

2017). The obtained OSL results reveal an underestimated age (10.2 ± 1.6 ka, GdTL-4618) compared to other results (**Table 1** and **2**). Three OSL dating results range from 11.6 ± 3.5 ka (GdTL-4611) to 11.9 ± 3.2 ka (GdTL-4615) (**Fig. 3**). These results are inconsistent with radiocarbon dating results from the peat below and two results from lower palaeosol above (14549 ± 65 calBP and 14500 ± 200 calBP, see **Fig. 3**). The dated quartz is generally characterised by a unimodal distribution of OSL measurements, which indicates sufficient extinction of the luminescence signal. Therefore, it is assumed that such discrepancies in dating results are not due to sedimentary processes but are the result of postdepositional processes. In this case, we assume that due to the good correlation of the radiocarbon dating results with previous studies (see **Fig. 2**), the deposition of this sediment series took place circa 16–14 ka ago (on the turn of the Late Pleniglacial and beginning of the Bølling interstadial).

Directly on the overbank deposits is located fluvio-aeolian complex (**Fig. 3**). It reflects the change of sedimentary processes and start of the river incision and abandonment of the floodplain. On the floodplain surface aeolian sands and silts were accumulated on dry (horizontal lamination) and wet (adhesion ripples) surface (Schwan, 1986; Kasse, 2002). The presence of small deformations as well as ice-wedge pseudomorphs reported in previous studies suggest severe climate conditions and presence at least of discontinuous permafrost (Zieliński *et al.*, 2015, 2019). The OSL dating results from the fluvio-aeolian complex (**Fig. 3**) are younger than radiocarbon dating results from the palaeosol above but older than TL dating results reported previously. Therefore, we assume that sedimentation took place in more or less the same time like in the upper part of the fluvial complex – the very end of the Late Pleniglacial and first part of the Bølling interstadial.

Amelioration of the climate conditions in the Bølling interstadial gave an impulse for development of soil processes and formation of the lower palaeosol (**Fig. 3**). The limited thickness, discontinuous strings of organic material as well as gleyic character is characteristic for palaeosols of the Bølling in Poland and suggests gradual melting of the permafrost below (Manikowska, 2002; Konecka-Betley, 2012). The lower palaeosol might be correlated with the palaeosol reported by Nowaczyk (1986).

Soil processes were interrupted by start of aeolian deposition of horizontally stratified sand cover. It was the result of ongoing river incision, formation of sandy terrace and release of overdried sands from it. A migration of sand transported by wind towards the east covered pre-existed soil. Local increase of moisture led to deposition of siltier unit reworked by soil processes (upper palaeosol, **Fig. 3**). Two OSL dating results from aeolian sand cover suggests short-distance transport and partial bleaching of sand. Presumably older OSL data (11.6 ± 3.5 ka, GdTL-4611) is unbleached and only younger OSL result (11.1 ± 1.0 ka, GdTL-4612) reveals more reliable age of deposition.

The upper palaeosol is of Gleysol type, similarly to the lower palaeosol. We assume therefore the same sedimentary process of silt deposition on the wet surface and the start of initial soil processes. Radiocarbon dating result from the palaeosol seems to be overestimated (16896 ± 55 calBP, GdA-6039) and suggests redeposition of the organic material from the infill of the abandoned channel in the direct vicinity of the studied profile due to deflation processes. Such possibility confirms the presence of several next organic infills in the study area of the Late Pleniglacial age (Nowaczyk, 1986; Bohnkce *et al.*, 1995). The palaeochannels not covered with aeolian deposits were further filled with organic material at least to the Early Holocene (Bohncke *et al.*, 1995).

The final stage of sedimentary processes is visible in the migrating towards the east parabolic dunes. The increase of available sand from the terraces was blown-out and formed complex dunes (Łopuch *et al.*, 2023). Obtained OSL dating results have wide range from 14.5 ± 1.2 ka (GdTL-4607) to 10.9 ± 1.3 ka (GdTL-4609) and reveal inversion (**Fig. 3**). It reduces their potential to proper location of the depositional processes on geological time scale. According to previous studies of the Late Glacial dune fields in Poland we assume that dunes formed in the Younger Dryas (Nowaczyk, 1986; Jankowski, 2012; Moska *et al.*, 2023). The TL dating results from the Żabinko site (Zieliński *et al.;* 2011, 2015) seems to be too young. However, reactivation of aeolian processes in the Holocene may not be excluded.

5. Conclusions

In conclusion, our study on the Żabinko site has provided valuable insights into its geological and chronological characteristics. The implementation of two independent dating methods, along with comparisons to previous studies and additional analyses, has allowed us to draw the following conclusions.

- Firstly, it was possible to determine the age of the studied succession; however, establishing a clear chronostratigraphy for the Żabinko site has proven challenging. The use of ^{14}C dating results compared to previous ones resulting in general stratigraphic model consistent with other results as well as allowed the correlation with previous results and cutting-edge results.
- The stratigraphic model obtained suggests an earlier onset of fluvial processes than previously assumed and progressive aggradation on the flood plain at the beginning of the late Pleniglacial and the beginning of the Late Glacial.
- The presence of disequilibrium was confirmed through activities of ^{234}Th, ^{226}Ra, and ^{210}Pb, as well as radon emanation measurements. This indicates that the investigated site exhibits variations in the radioactive decay series.
- The analysis revealed non-homogeneity of the material at the Żabinko site. Laminations observed in the profile

suggest the presence of heterogeneous sediment layers. This finding highlights the importance of considering material non-homogeneity in the dose rate measurements.

- The occurrence of numerous additional physical and geological factors, such as changes in groundwater levels and chemical weathering, might be considered as influential factors affecting the determination of dose rates. These factors could contribute to the variability observed in the dating results.
- In future investigations, it is essential to assess the homogeneity of the material collected at the Żabinko site and evaluate the variation in dose rates among samples located in close proximity to each other. This will provide further insights into the spatial distribution of chronologically relevant parameters and contribute to the refinement of the chronostratigraphy for the site.

Overall, our study emphasizes the need for comprehensive investigations that consider multiple dating methods, compare results with other researchers, and account for the effects of disequilibrium and material non-homogeneity. These considerations occurred to be crucial for establishing chronology in a such complex geological setting like the Żabinko site.

Acknowledgements

The presented results were obtained with the support of the Polish National Science Centre, contract numbers: 2018/30/E/ST10/00616, 2021/41/N/ST10/00169 and with the support for young scientists in the Division of Geochronology and Environmental Isotopes, 2023: 14/020/BKM/0037.

References

Aitken MJ, 1985. *Thermoluminescence Dating*. London, Academic Press, 359 pp.

Autzen M, Andersen CE, Bailey M and Murray AS, 2022. Calibration quartz: An update on dose calculations for luminescence dating. *Radiation Measurements* 157: 106828, DOI 10.1016/j.radmeas.2022.106828.

Bateman MD, 2008. Luminescence dating of periglacial sediments and structures. *Boreas* 37: 574–588, DOI 10.1111/j.1502-3885.2008.00050.x.

Bell WT, 1979. Attenuation Factors for the Absorbed Radiation Dose in Quartz Inclusions for Thermoluminescence Dating. *Ancient TL* (8): 2–13.

Benito G, Sánchez-Moya Y and Sopeña A, 2003. Sedimentology of high-stage flood deposits of the Tagus River, Central Spain. *Sedimentary Geology* 157: 107–132, DOI 10.1016/S0037-0738(02)00196-3.

Bohncke S, Kasse C and Vanderberghe J, 1995. Climate induced environmental changes during the Vistulian Lateglacial at Żabinko, Poland. *Questiones Geographicae, Special Issue* 4: 43–64.

Brauer A, Hajdas I, Blockley SP, Bronk Ramsey C, Christl M, Ivy-Ochs S, Moseley GE, Nowaczyk NN, Rasmussen SO, Roberts HM and Spötl C, 2014. The importance of independent chronology in integrating records of past climate change for the 60–8 ka INTIMATE time interval. *Quaternary Science Reviews* 106: 47–66, DOI 10.1016/j.quascirev.2014.07.006.

Brennan BJ, 2003. Beta doses to spherical grains. *Radiation Measurements* 37(4–5): 299–303, DOI 10.1016/S1350-4487(03)00011-8.

Brennan BJ, Lyons R and Phillips SW, 1991. Attenuation of alpha particle track dose for spherical grains. *International Journal of Radiation Applications and Instrumentation. Part D. Nuclear Tracks and Radiation Measurements* 18(1–2): 249–253, DOI 10.1016/1359-0189(91)90119-3.

Bronk Ramsey C, 2009. Bayesian analysis of radiocarbon dates. *Radiocarbon* 51: 337–360, DOI 10.1017/S0033822200033865.

Burns CE, Mountney NP, Hodgson DM and Colombera L, 2017. Anatomy and dimensions of fluvial crevasse-splay deposits: examples from the Cretaceous Castlegate sandstone and Neslen formation, Utah, USA. *Sedimentary Geology* 351: 21–35, DOI 10.1016/j.sedgeo.2017.02.003.

Crombé P, Bos JA, Cruz F and Verhegge J, 2020. Repeated aeolian deflation during the Allerød/GI-1a-c in the coversand lowland of NW Belgium. *Catena* 188: 104453, DOI 10.1016/j.catena.2020.104453.

Cutshall NH, Larsen IL and Olsen CR, 1983. Direct analysis of 210Pb in sediment samples: Self-absorption corrections. *Nuclear Instruments and Methods in Physics Research* 206: 309–312, DOI 10.1016/0167-5087(83)91273-5.

FAO, 1988. FAO/Unesco Soil Map of the World, Revised Legend, with corrections. Word Resources Report 60, FAO, Rome.

Fitzsimmons KE, Rhodes EJ, Magee JW and Barrows TT, 2007. The timing of linear dune activity in the Strzelecki and Tirari Deserts, Australia. *Quaternary Science Reviews* 26: 2598–2616, DOI 10.1016/j.quascirev.2007.06.010.

Galbraith RF, Roberts RG, Laslett GM, Yoshida H and Olley JM, 1999. Optical dating of single and multiple grains of quartz from Jinmium Rock Shelter, Northern 12 Australia. Part I, experimental design and statistical models. *Archaeometry* 41: 1835–1857, DOI 10.1111/j.1475-4754.1999.tb00988.x.

Gradziński R, Baryła J, Doktor M, Gmur D, Gradziński M, Kędzior A, Paszkowski M, Soja R, Zieliński T and Żurek S, 2003. Vegetation-controlled modern anastomosing system of the upper Narew River (NE Poland) and its sediments. *Sedimentary Geology* 157: 253–276, DOI 10.1016/S0037-0738(02)00236-1.

Guérin G, Mercier N and Adamiec G, 2011. Dose-rate conversion factors: update. *Ancient TL* 29: 5–8.

Hughes A, Gyllencreutz R, Lohne ØS, Mangerud J and Svendsen JI, 2016. The last Eurasian ice sheets–a chronological database and time-slice reconstruction, DATED-1. *Boreas* 45: 1–45, DOI 10.1111/bor.12142.

Jankowski M, 2012. Lateglacial soil paleocatena in inland-dune area of the Toruń Basin, Northern Poland. *Quaternary International* 265: 116–125, DOI 10.1016/j.quaint.2012.02.006.

Kalińska E, Weckwerth P and Alexanderson H, 2023. Recent advances in luminescence dating of the Late Quaternary sediments in the Baltic States, Northern Europe: A review. *Earth-Science Reviews* 236: 104272, DOI 10.1016/j.earscirev.2022.104272.

Kasse C, 2002. Sandy aeolian deposits and their relation to climate during the Last Glacial Maximum and Lateglacial in northwest and central Europe. *Progress in Physical Geography: Earth and Environment* 26: 507–532, DOI 10.1191/0309133302pp350ra.

Konecka-Betley K, 2012. Late Glacial and Holocene 14 C-dated fossil soils in the Middle Vistula Valley. *Soil Science Annual* 63(4): 50–60, DOI 10.2478/v10239-012-0041-0.

Kozarski S, Gonera P and Antczak B, 1988. Valley floor development and paleohydrological changes: the Late Vistulian and Holocene history of the Warta river (Poland). [In:] Lang, G., Schluchter, C. (Eds), Lake, Mire and River Environments During the Last 15 000 Years. *Balkema* 185–203.

Kozarski S and Nowaczyk B, 1995. The Bólling interstadial at Żabinko and Late Vistulian environmental changes in middle reach of the Warsaw-Berlin Pradolina. *Quaternary Studies in Poland* 13: 43–53.

Łopuch M, Sokołowski RJ and Jary Z, 2023. Factors controlling the development of cold-climate dune fields within the central part of the European Sand Belt – insights from morphometry. *Geomorphology* 420: 108514. DOI 10.1016/j.geomorph.2022.108514.

Manikowska B, 2002. Fossil paleosols and pedogenetic periods in the evolution of Central Poland environment after the Wartian Glaciation. In: Manikowska, B. Konecka-Betley, K., Bednarek, R., (Eds.), *Paleopedology problems in Poland*. ŁTN, Łódź, 165–212.

Mason JA, Jacobs PM, Greene RSB and Nettleton WD, 2003. Sedimentary aggregates in the Peoria Loess of Nebraska, USA. *Catena* 53: 377–397, DOI 10.1016/S0341-8162(03)00073-0.

Miall AD, 1996. The Geology of Fluvial Deposits: Sedimentary Facies, Basin Analysis and Ptreoleum Geology. *Springer-Verlag*, New York, pp. 1–582.

Moska P, 2019. Luminescence dating of Quaternary sediments – some practical aspects. *Studia Quaternaria* 36: 2161–2169, DOI 10.24425/sq.2019.126387.

Moska P, Bluszcz A, Poręba G, Tudyka K, Adamiec G, Szymak A and Przybyła A, 2021. Luminescence dating procedures at the Gliwice Luminescence Dating Laboratory. *Geochronometria* 48: 1–15, DOI 10.2478/geochr-2021-0001.

Moska P, Sokołowski RJ, Jary Z, Zieliński P, Raczyk J, Szymak A, Krawczyk M, Skurzyński J, Poręba G, Łopuch M and Tudyka K, 2022. Stratigraphy of the Late Glacial and Holocene aeolian series in different sedimentary zones related to the Last Glacial maximum in Poland. *Quaternary International* 630: 65–83, DOI 10.1016/j.quaint.2021.04.004.

Moska P, Sokołowski RJ, Zieliński P, Jary Z, Raczyk J, Mroczek P, Szymak A, Krawczyk M, Skurzyński J, Poręba G, Łopuch M and Tudyka K, 2023. An Impact of Short-Term Climate Oscillations in the Late Pleniglacial and Lateglacial Interstadial on Sedimentary Processes and the Pedogenic Record in Central Poland, *Annals of the American Association of Geographers* 113: 46–70, DOI 10.1080/24694452.2022.2094325.

Murray AS and Wintle AG, 2000. Luminescence dating of quartz using an improved single aliquot regenerative-dose protocol. *Radiation Measurements* 32: 57–73, DOI 10.1016/S1350-4487(99)00253-X.

Nowaczyk B, 1986. Wiek wydm, ich cechy granulometryczne i strukturalne a schemat cyrkulacji atmosferycznej w Polsce w późnym vistulianie i holocenie (The age of dunes, their textural and structural properties against atmospheric circulation pattern of Poland during the Late Vistulian and Holocene). Seria Geografia 28. Poznań, Wyd. Naukowe UAM: 245pp (in Polish)

Pincé P, Vandenberghe D, Moayed NK, De Dapper M, Debeer AE, Van Maldegem E, Verhegge J, Piret L, De Grave J and Crombé P, 2022. High-resolution OSL chronology of a well-preserved inland dune in the Lys valley (Sint-Martens-Latem, NW Belgium). *Quaternary Geochronology* 72: 101322, DOI 10.1016/j.quageo.2022.101322.

Poręba G, Tudyka K, Szymak A, Pluta J, Rocznik J, Świątkowski J, Osadnik R and Moska P, 2022. Evaluating the effect of hydrofluoric acid etching on quartz grains using microscope image analysis, laser diffraction and weight loss particle size estimate. *Geochronometria* 49: 1–8, DOI 10.2478/geochr-2022-0001.

Poręba G, Tudyka K, Walencik-Łata A and Kolarczyk A, 2020. Bias in ^{238}U decay chain members measured by γ-ray spectrometry due to 222Rn leakage. *Applied Radiation and Isotopes* 156: 108945, DOI 10.1016/j.apradiso.2019.108945.

Prescott JR and Hutton JT, 1994. Cosmic ray contributions to dose rates for luminescence and ESR dating, large depths and long-term variations. *Radiation Measurements* 23: 497–500, DOI 10.1016/1350-4487(94)90086-8.

Rasmussen SO, Bigler M, Blockley SP, Blunier T, Buchardt SL, Clausen HB, Cvijanovic I, Dahl-Jensen D, Johnsen SJ, Fischer H, Gkinis V, Guillevic M, Hoek WZ, Lowe JJ, Pedro JB, Popp T, Seierstad IK, Steffensen JP, Svensson AM, Vallelonga P, Vinther BM, Walker MJC, Wheatley JJ, Winstrup M, 2014. A stratigraphic framework for abrupt climatic changes during the Last Glacial period based on three synchronized Greenland ice-core records: refining and extending the INTIMATE event stratigraphy. *Quaternary Science Reviews* 106: 14–28, DOI 10.1016/j.quascirev.2014.09.007.

Reimer P, Austin W, Bard E, Bayliss A, Blackwell P, Bronk Ramsey C, Butzin M, Cheng H, Edwards R, Friedrich M, Grootes P, Guilderson T, Hajdas I, Heaton T, Hogg A, Hughen K, Kromer B, Manning S, Muscheler R, Palmer J, Pearson C, van der Plicht J, Reimer R, Richards D, Scott E, Southon J, Turney C, Wacker L, Adolphi F, Büntgen U, Capano M, Fahrni S, Fogtmann-Schulz A, Friedrich R, Köhler P, Kudsk S, Miyake F, Olsen J, Reinig F, Sakamoto M, Sookdeo A and Talamo S, 2020. The IntCal20 Northern Hemisphere radiocarbon age calibration curve (0–55 cal kBP). *Radiocarbon* 62: 725–757, DOI 10.1017/RDC.2020.41.

Sanderson DCW, 1988. Thick source beta counting (TSBC): A rapid method for measuring beta dose-rates. *International Journal of Radiation Applications and Instrumentation*. *Part D. Nuclear Tracks and Radiation Measurements* 14(1–2): 203–207, DOI 10.1016/1359-0189(88)90065-9.

Schwan J, 1986. The origin of horizontal alternating bedding in Weichselian Aeolian sands in northwestern Europe. *Sedimentary Geology* 49: 73–108, DOI 10.1016/0037-0738(86)90016-3.

Sokołowski RJ, Moska P, Zieliński P, Jary Z, Piotrowska N, Raczyk J, Mroczek P, Szymak, A, Krawczyk M, Skurzyński J, Poręba G, Łopuch M and Tudyka K, 2022. Reinterpretation of fluvio-aeolian succession from Late Glacial classic type localities using new high-resolution radiocarbon dating results from the Polish part of the European Sand Belt. *Radiocarbon* 64: 1387–1402, DOI 10.1017/RDC.2022.37.

Strong KP and Levins DM, 1982. Effect of Moisture Content on Radon Emanation from Uranium Ore and Tailings. *Health Physics* 42(1): 27–32, DOI 10.1097/00004032-198201000-00003.

Szymak A, Moska P, Poręba G, Tudyka K and Adamiec G, 2022. The internal dose rate in quartz grains: experimental data and consequences for luminescence dating. *Geochronometria* 49: 9–17, DOI 10.2478/geochr-2022-0002.

Tudyka K, Miłosz S, Adamiec G, Bluszcz A, Poręba G, Paszkowski Ł and Kolarczyk A, 2018. µDose: A compact system for environmental radioactivity and dose rate measurement. *Radiation Measurements* 118: 8–13, DOI 10.1016/j.radmeas.2018.07.016.

Tudyka K, Koruszowic M, Osadnik R, Adamiec G, Moska P, Szymak A, Bluszcz A, Zhang J, Kolb T and Poręba G, 2022. µRate: An online dose rate calculator for trapped charge dating. *Archaeometry* 65: 423–443, DOI 10.1111/arcm.12828.

Zeeberg J, 1998. The European sand belt in eastern Europe — and comparison of Late Glacial dune orientation with GCM simulation results. *Boreas* 27(2): 127–139, DOI 10.1111/j.1502-3885.1998.tb00873.x.

Zieliński P, 2016. Regionalne i lokalne uwarunkowania późnovistuliańskiej depozycji eolicznej w środkowej części europejskiego pasa piaszczystego [Regional and local conditions of the Late Vistulian aeolian deposition in the central part of the European Sand Belt]. *Wydawnictwo UMCS*. Lublin 1–235 [in Polish with English summary].

Zieliński P, Sokołowski RJ, Fedorowicz S and Jankowski M, 2011. Stratigraphic position of fluvial and aeolian deposits in the Żabinko site based on TL dating. *Geochronometria* 38: 64–71, DOI 10.2478/s13386-011-0005-x.

Zieliński P, Sokołowski RJ, Woronko B, Jankowski M, Fedorowicz S, Zaleski I, Molodkov A and Weckwerth P, 2015. The depositional conditions of the fluvio-aeolian succession during the last climate minimum based on the examples from Poland and NW Ukraine. *Quaternary International* 386: 30–41, DOI 10.1016/j.quaint.2014.08.013.

Zieliński P, Sokołowski RJ, Jankowski M, Standzikowski K and Fedorowicz S, 2019. The climatic control of sedimentary environment changes

during the Weichselian–An example from the Middle Vistula Region (eastern Poland). *Quaternary International* 501: 120–134, DOI 10.1016/j.quaint.2018.04.036.

Zieliński T, 1998. Litofacjalna identyfikacja osadów rzecznych [Lithofacial identification of alluvial sediments]. In: Mycielska-Dowgiałło, E. (Ed.), Struktury Sedymentacyjne i Postsedymentacyjne W Osadach Czwartorzędowych [Sedimentary and Postsedimentary Structures in Quaternary Sediments and Their Value for Interpretation]. *University of Warsaw Press*, pp. 195–260 [in Polish with English summary].

Zieliński T, 2014. Sedymentologia. Osady rzek i jezior [Sedimentology. Deposits of rivers and lakes]. *Wydawnictwo Naukowe* UAM. Poznań 1–594 [in Polish].